International Journal of Computer Information Systems and Industrial Management Applications
ISSN 2150-7988 Volume 3 (2011) pp. 371-390

A Novel Approach to Predict Earthquakes using Adaptive Neural Fuzzy Inference System and Conservation of Energy-Angular Momentum

Murad Shibli

Visiting Assistant Professor, *Mechanical Engineering Department,*
College of Engineering, United Arab Emirates University, P.O. Box 15551, Al-Ain, UAE
Tel.: 971-509328707,malshibli@uaeu.ac.ae

Abstract: **This paper presents an adaptive neural fuzzy inference system (ANFIS) approach to predict the location, occurrence time and the magnitude of earthquakes. The analysis conducted in this paper is based on the principle of conservation of energy and momentum of annual earthquakes which has been validated by analyzing data obtained from United Sates Geographical Survey (USGS). This principle shall not be violated due to the fact that the angular earth speed about its axis is fixed to keep the 24 hours daytime unchanged. Furthermore, it is assumed that the area under the moment curve of earthquakes in the north part of the earth balances the area under the moment curve in the south part of the earth due to the conservation principle. For automatically tuning Sugeno-type inference systems, a sample of training data is used to train the ANFIS system using 3 bell-shape membership functions with grid partition to generate the fuzzy inference system (FIS) along with 270 epochs. In training the earthquake ANFIS methodology, the location of the earthquake is used as an input, meanwhile the moment of the earth quake is assigned as the output. The resulted training error was stabilized after 250 epochs converging to an acceptable value of 0.84. To further enhance prediction of earthquakes, different data set is used to verify the validity of ANFIS output. The inputs to ANFIS are the latitude, longitude and date to predict the corresponding earthquake moments as an output. Surprisingly, the FIS system is found to be capable to predict most of the earthquakes moment-magnitude at the specified location with a 0.17424 converging error. Dynamic ANFIS earthquake predictor along with 3D meshed surfaces are found to be efficient as well. Finally, the ANFIS results are demonstrated to show the effectiveness of the approach.**

Keywords: Earthquakes, prediction of earthquakes, ANFIS, Fuzzy, Neural Networks, Conservation Energy-Momentum

I. Introduction

One of the most frightening and destructive phenomena of nature is a severe earthquake and its terrible aftereffects [1]. An earthquake is a sudden movement of the Earth, caused by the abrupt release of strain that has accumulated over a long time. For hundreds of millions of years, the forces of plate tectonics have shaped the Earth as the huge plates that form the Earth's surface slowly move over, under, and past each other. Sometimes the movement is gradual. At other times, the plates are locked together, unable to release the accumulating energy. When the accumulated energy grows strong enough, the plates break free. If the earthquake occurs in a populated area, it may cause many deaths and injuries and extensive property damage.

Today we are challenging the assumption that earthquakes must present an uncontrollable and unpredictable hazard to life and property. Scientists have begun to estimate the locations and likelihoods of future damaging earthquakes. Sites of greatest hazard are being identified, and definite progress is being made in designing structures that will withstand the effects of earthquakes [1].

The article [2] presents a method of monitoring earthquake activity on the planetary scale using the data of all individual earthquakes on Earth since 1973, available from US Geological Survey (USGS). The method reveals that in recent years the annual earthquake energy on Earth has increased five times and that its trend is to grow in the future. Statistics has been made for the whole area of Japan and its neighborhood [3]. If the area is divided into several units and each of the units is investigated separately, the uniformity of energy release does not show up. A certain size of area appears to be necessary for the uniformity of energy release to be established. Whether or not this size differs in various seismic regions of the world is an important problem to be studied. The energy release in great earthquakes is presented in [4]. A new earthquake magnitude scale is proposed in terms of the standard energy-magnitude relation as large as 9.5 and for earth rupture magnitude of about 100 km or less. A great 8.8-magnitude struck central Chile in January 2010 [5]. The quake hit 200 miles (325 kilometers) southwest of the capital Santiago.

The epicenter was just 70 miles (115 kilometers) from Concepcion, Chile's second-largest city.

Relationships among magnitudes and seismic moment of earthquakes in the Taiwan region is introduced in [6]. Three relationships have high agreement with those of earthquakes in the circum-Pacific seismic belt. This might imply that the tectonic conditions and source properties of the Taiwan region behave like the average ones of the circum-Pacific seismic belt. Fuzzy risk assessment on earthquake hazard on city is presented in [7]. A Fuzzy mathematical method of Urban Natural Hazard and Risk Assessment is introduced.

The architecture and learning procedure underlying ANFIS is presented in [8], which is a fuzzy inference system implemented in the framework of adaptive networks. By using hybrid learning procedure, the proposed ANFIS can construct an input-output mapping based on human knowledge (in the from of fuzzy if-then rules) and stipulated input-output data pairs. In simulation, the ANFIS architecture is employed to model nonlinear functions, , identify nonlinear components on-linearly in a control system, and predict a chaotic time series, all yielding remarkable results. Comparisons with artificial neural networks and earlier work on fuzzy modeling are listed and discussed. Other extensions of the proposed ANFIS and promising applications to automatic control and signal processing are also suggested.

Recent years have seen a rapidly growing number of hybrid Adaptive Neural Fuzzy Inference System based applications in the process engineering field, estimation, modeling and control systems among others. This paper presents the application of an adaptive network based fuzzy inference system (ANFIS) predictor is to the estimation of earthquakes in terms of magnitude, location and its expected timing occurrence. Basically, a fuzzy controller is composed of a rule base containing fuzzy if-then rules. A database with membership functions of the fuzzy sets, an inference engine and two fuzzification and defuzzification interfaces to convert crisp inputs into degrees of match with linguistic values and vice versa. An ANFIS system (Adaptive Neural Fuzzy Inference System) is a kind of adaptive network in which each node performs a particular function of the incoming signals, with parameters updated according to given training data and a gradient-descent learning procedure [8]. This paper is organized as follows. Section 2 introduces the fundamentals of ANFIS. In section 3, scaling earthquake magnitude, energy and moment is detailed. Meanwhile, section 4 presents the training data used for ANFIS and the corresponding results. Finally, conclusions and future work are summarized.

II. Adaptive Neural Fuzzy Inference System

An ANFIS system is a kind of adaptive network in which each node performs a particular function of the incoming signals, with parameters updated according to given training data and a gradient-descent learning procedure. This hybrid architecture has been applied to the modeling and control of multiple-input single-output (MISO) systems [8-9].

The architecture of the ANFIS is constituted by several layers as shown in Figure 1. If we consider for simplicity two inputs x and y and two outputs f_1 and f_2 for a first-order Sugeno fuzzy model, with A_i and B_j being the linguistic label associated with x and y respectively, every node in layer 1 represents a bell-shaped membership function $\mu_{A_i}(x)$ or $\mu_{B_i}(y)$ with variable membership parameters. Commonly choose the bell-shaped functions are chosen. Nodes of layer 2 output the firing strength defined as the product $\omega_{ji} = \mu_{A_i}(x) \times \mu_{B_i}(y)$, where the set of nodes in this layer are grouped for each output j. A normalization process is computed in layer 3 giving the normalized $\overline{\omega}_{ji}$, and the Sugeno-type consequent of each rule with variable parameters p_i, q_i and r_i is implemented in layer 4 yielding f_j as the output of the single summation node $f_i = \sum_i \overline{\omega}_{ji(} p_i x + q_i y + r_i)$ and finally the single node of layer 5 computes de overall output as a summation of all incoming signals. The learning procedure consists of two stages. In the forward pass training input data go forward the ANFIS architecture, and in the backward pass the error rates propagate backward, being the both the consequent and the membership parameters updated by gradient descent.

A Two Rule Sugeno ANFIS has rules of the form:

$$If\ x\ is\ A_1\ and\ y\ is\ B_1 \quad THEN\ f_1 = p_1 x + q_1 y + r_1$$
$$If\ x\ is\ A_2\ and\ y\ is\ B_2 \quad THEN\ f_2 = p_2 x + q_2 y + r_2 \tag{1}$$

ANFIS Architecture: The ANFIS architecture is described as follows:

__Layer 1__: Adaptive Nodes

$$O_{1,i} = \mu_{A_i}(x), \quad i = 1, 2$$
$$O_{1,i} = \mu_{B_{i-2}}(y), \quad i = 3, 4 \tag{2}$$

$\mu_{A_i}(x)$ and $\mu_{B_i}(y)$: any appropriate parameterized membership functions of x and y.

$\mu_{A_i}(x) = \dfrac{1}{1 + [\frac{(x - c_i)^2}{a_i^2}]^{b_i}}$. A special form is the bell-shaped function described by the membership function

$$\mu_A(x) = \frac{1}{1+\left|\frac{x-c_i}{a_i}\right|^{2b_i}} \quad (3)$$

where the set $\{a_i, b_i, c_i\}$ are the premise parameters.

<u>Layer 2</u>: Contains fixed nodes with function of multiplication where the t-norm is used to 'AND' the membership grades such as:

$$O_{2,i} = w_i = \mu_{A_i}(x) \times \mu_{B_i}(x) \qquad i = 1,\ 2 \quad (4)$$

are the firing strength of a given rule.

<u>Layer 3</u>: Composed fixed nodes with function of normalization to calculate the ratio of the firing strengths of the rules such that

$$O_{3,i} = \overline{w}_i = \frac{w_i}{w_1 + w_2}, \quad i = 1, 2 \quad (5)$$

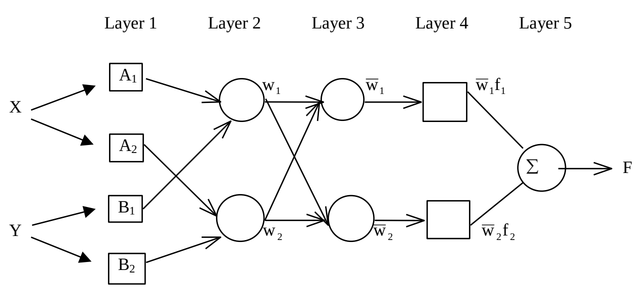

Figure 1: Architecture of the ANFIS Network Structure

<u>Layer 4</u>: The nodes in this layer are adaptive and perform the consequent of the rules to:

$$O_{4,i} = overall output = \overline{w}_i f_i = \overline{w}_i (p_i x + q_i y + r_i) \quad (6)$$

where $\{p_i, q_i, t_i\}$ are the consequent parameters to be estimated.

<u>Layer 5</u>: There is a single node here that computes the overall output

$$O_{5,i} = \sum_i \overline{w_i} f_i = \frac{\sum_i w_i f_i}{\sum_i w_i} \quad (7)$$

Hybrid Learning Algorithm: when the premise parameters are fixed such that:

$$f = \frac{w_1}{w_1 + w_2} f_1 + \frac{w_2}{w_1 + w_2} f_2 = \overline{w}_1 f_1 + \overline{w}_2 f_2$$
$$= (\overline{w}_1 x) p_1 + (\overline{w}_1 y) q_1 + (\overline{w}_1) r_1 + (\overline{w}_2 x) q_2 + (\overline{w}_2 y) q_2 + (\overline{w}_2) r_2 \quad (8)$$

are called the linear function of consequent parameters.

III. Scaling Earthquake Magnitude, Energy and Moment

A Fault is basically a big crack in the earth's crust. They can be either shallow or deep but the deformation of the rock around them is something all faults have in common. Faults are the most visible evidence of seismic activity. That is why they are so useful in helping scientist determine plate boundaries and regions that experience geological activity. Major seismic activity such as earthquakes are result of energy being released when a fault slips. This is why cities like San Francisco are at risk for earthquakes.

Faults are caused when seismic activity causes stress on a layer of rock causing it to fracture then slip against itself. There are three main types of faults. The first type of fault is a dip slip fault. This is a fault that occurs where one side of a rock fracture is pushed over or beneath the other. These can be either reverse or normal. The next type of fault is the strike slip. This one is completely horizontal with little up or down movement. Instead to the two sides of the fault slip past each other horizontally. The third major type is the oblique slip fault. It is sort of a combination of both a strike slip and a dip slip fault. There are other less common types of faults such as ring faults and lispic faults. There are more circular in shape.

A. *Earthquakes and Earth Day Shortening/Lengthening*

By speeding up Earth's rotation, it has been estimated that the magnitude 8.8 2010 earthquake in Chile (the fifth strongest ever recorded, according to the USGS) may have affected the entire planet by shifting Earth on its axis. This possibly may have shortened the length of a day on Earth by about 1.26 microseconds. Using a complex model JPL research scientist Richard Gross computed how Earth's rotation should have changed as a result of the Feb. 27, 2010 earthquake [12]. Based on this model, the quake should have moved Earth's figure axis (the axis about which Earth's mass is balanced) by 2.7 milliarcseconds (about 8 centimeters, or 3 inches).

The day duration T is related to the Earth's rotation speed ω is simply expressed as

$$T = \frac{2\pi}{\omega} \quad (9)$$

To express the shortening or lengthening of the day duration as follows

$$\Delta T = \frac{2\pi}{\Delta\omega} \quad (10)$$

B. Earthquakes and Conservation of Angular Momentum of Earth

During earthquakes, the ground shakes as tectonic plates shift along a fault line. Tectonic plates can move horizontally or vertically. Either way masses of rock in Earth's crust change location and accordingly the mass distribution in Earth's crust changes. The law of conservation of angular momentum requires that the total angular momentum of a system P with no external torques (rotational forces) remains constant. Analogous to linear momentum being mass multiplied by velocity, angular momentum is moment of inertia I multiplied by angular velocity ω as follows:

$$P = I \times \omega = const. \tag{11}$$

In order to keep the angular momentum constant, if the moment of inertia increases, the angular velocity decreases. If however the moment of inertia decreases, the angular velocity increases. The moment of inertia of a point mass is its mass multiplied by the square of its distance from the rotation axis. For distribution of extended mass, the total moment of inertia is the total of the moments of inertia for each point in the mass distribution.
Now the change in the day duration now can be modified as

$$\Delta T = 2\pi \frac{\Delta I}{P} \tag{12}$$

As an earthquake shifts rock in Earth's crust; it changes how Earth's mass is distributed. Earthquakes that move tectonic plates vertically change the distance of the tectonic plate from Earth's rotational axis. This small distance change affects Earth's moment of inertia, which will in turn change, ever so slightly, Earth's rotation rate. If part of a tectonic plate moves downward, its distance from Earth's rotational axis decreases. Earth's moment of inertia decreases. Earth's angular velocity increases to conserve angular momentum. As Earth spins faster, the day length shortens an imperceptible amount. If the tectonic plate moves upward, the opposite occurs and the day gets longer.

The day got shorter after the major earthquakes in 2010 and 2004 because tectonic movements shifted some mass closer to Earth's rotation axis, decreased Earth's moment of inertia, and increased Earth's rotation rate. Deviating roughly 33 feet (10 meters) from the north-south axis around which Earth revolves, the figure axis is the imaginary line around which the world's unevenly distributed mass is balanced. By comparison, the same model estimated the 2004 magnitude 9.1 Sumatran earthquake should have shortened the length of day by 6.8 microseconds and shifted Earth’s axis by 2.32 milliarcseconds (about 7 centimeters, or 2.76 inches).

Even though the Chilean earthquake is much smaller than the Sumatran quake, it is predicted to have changed the position of the figure axis by a bit more for two reasons. First, unlike the 2004 Sumatran earthquake, which was located near the equator, the 2010 Chilean earthquake was located in Earth’s mid-latitudes, which makes it more effective in shifting Earth’s figure axis. Second, the fault responsible for the 2010 Chiliean earthquake dips into Earth at a slightly steeper angle than does the fault responsible for the 2004 Sumatran earthquake. This makes the Chile fault more effective in moving Earth’s mass vertically and hence more effective in shifting Earth’s figure axis. Only thrust earthquakes, with their inward motion, can shorten Earth days. Other types of earthquakes, such as horizontal strike-slip quakes, in which two plates slide horizontally past one another, don't affect Earth's rotation. The recent Earth-axis jolt may have been the result of stress buildup from a magnitude 9.5 quake that struck Chile in 1960. It is quite similar to the December 26, 2004, magnitude 9.0 Sumatra earthquake, which was followed by a magnitude 8.7 quake on [the Sumatra fault's] southern end on the 28th of March 2005. Thus, the earthquake-interaction possibility seriously.

The Richter magnitude scale, also known as the local magnitude (M_L) scale, assigns a single number to quantify the amount of seismic energy released by an earthquake [1]. It is a base-10 logarithmic scale obtained by calculating the logarithm of the combined horizontal amplitude (shaking amplitude) of the largest displacement from zero on a particular type of seismometer (Wood–Anderson torsion). So, for example, an earthquake that measures 5.0 on the Richter scale has a shaking amplitude 10 times larger than one that measures 4.0. The effective limit of measurement for local magnitude M_L is about 6.8.

The Richter scale has been superseded by the moment magnitude scale, which is calibrated to give generally similar values for medium-sized earthquakes (magnitudes between 3 and 7). Unlike the Richter scale, the moment magnitude scale is built on sound seismological principles, and does not saturate in the high-magnitude range. The energy release of an earthquake, which closely correlates to its destructive power, scales with the $3/2$ power of the shaking amplitude. Thus, a difference in magnitude of 1.0 is equivalent to a factor of 31.6 (= $(10^{1.0})^{(3/2)}$) in the energy released; a difference in magnitude of 2.0 is equivalent to a factor of 1000 (= $(10^{2.0})^{(3/2)}$) in the energy released. The energy release of an earthquake can be determined if the magnitude is known using the Richter and Gutenberg Seismic Energy Formula:

$$\begin{gathered} Energy = 10^{(11.8+1.5*Magnitude)} \\ Magnitude = \frac{\log_{10}(Energy) - 11.8}{1.5} \end{gathered} \tag{13}$$

On the other hand, Seimic moment and magnitude relationship

$$\text{Magnitude} = \frac{2}{3} \times [\log_{10}(\text{Moment}) - 16.1]$$

$$\text{Moment} = 10^{(3/2 \times \text{Magnitude} + 16.1)} \quad (14)$$

Previous formulas have been used to analyze the energy and moment released by earthquakes based on their corresponding magnitude. Data obtained from USGS are used to investigate how frequent earthquakes occur and strong they are. Figure 2 demonstrates how frequent earthquakes are based on their magnitude. Looking at strong earthquakes with 8 or more magnitude they usually occur once a year. Meanwhile for magnitudes 7-7.9, 6-6.9 and 5-5.9, earth can witness 17,134 and 1319, respectively. Weak earthquakes with 2-2.9 are experienced daily up 13000 a year. Bu since 2-2.9 magnitude earthquake release low energy and thus cannot be felt by people. Being interested in energy generated by an earthquake would be maximum at 8-9 Magnitude with an energy fold of 4×10^{18} *Joules*.

This amount can be reduced to its half with a magnitude of 7-7.9. Moreover, such energy release can be reduced by a million manifold at 5-5.9 Magnitude. The minimum energy would occurs at 2-2.9 magnitude in the range of 10^{12} *Joules*. More details are shown in Figure 3. Looking at Figure 4, we can see that the number of major earthquakes ranges from 15 to 40 with an average of 20. Knowing how frequently earthquakes occur because of their catastrophic damage and deaths they might result in. On the hand, Figure 5 gives more details on the total number of earthquakes that jolt annually for the decade 1990-1999. It is figured out that the average is close 20,000 earthquakes a year. Similarly, Figure 5 shows the frequency of earthquakes for years 2000-2009. It is noticed that the total number of earthquakes has jumped to 30,000 as shown in Figure 6.

This shows that Erath has witnessed more activities in its tectonic plates. Further steps are needed to analyzed in the next figures in terms of as detailed in figures 5 and 6. Investigating the energy produced annually by an earthquake is now demonstrated in Figure 7 for years 1990-1999. For the first three years 1990-1993, the energy release is stable and in the range of 10^{17} *Joules*. This energy manifold has had been boomed by 10 times to 4×10^{18} *Joules*. Noticeably it had been dropped down in 1997 to same energy as was level 1990-1993.

The records of USGS shows an increase in earthquake for the new millennium activities for years 2000-2009 comparing to previous decade jumping from an average of 20000 to 30,000 as shown in Figure 8. Similarly, the energy manifold is magnified to the 10^{18} *Joules* range. The minimal recorded in year 2002 with 10^{17} *Joules* compared to a maximum in 2007 with 8.8×10^{18} *Joules*.

Some scientists refer this rise in earthquake activities to global warming and industrial activities. This ensures the how it is crucial to investigate more sophisticated approaches to predict earthquakes, its strengths, location and expected time of occurrence. Adaptive neural fuzzy inference system can deal with such a uncertainty of earthquakes and its nonlinearity behavior. Next section will classify the training data, basic input-output variables such as latitude, longitude, strength and time occurrence.

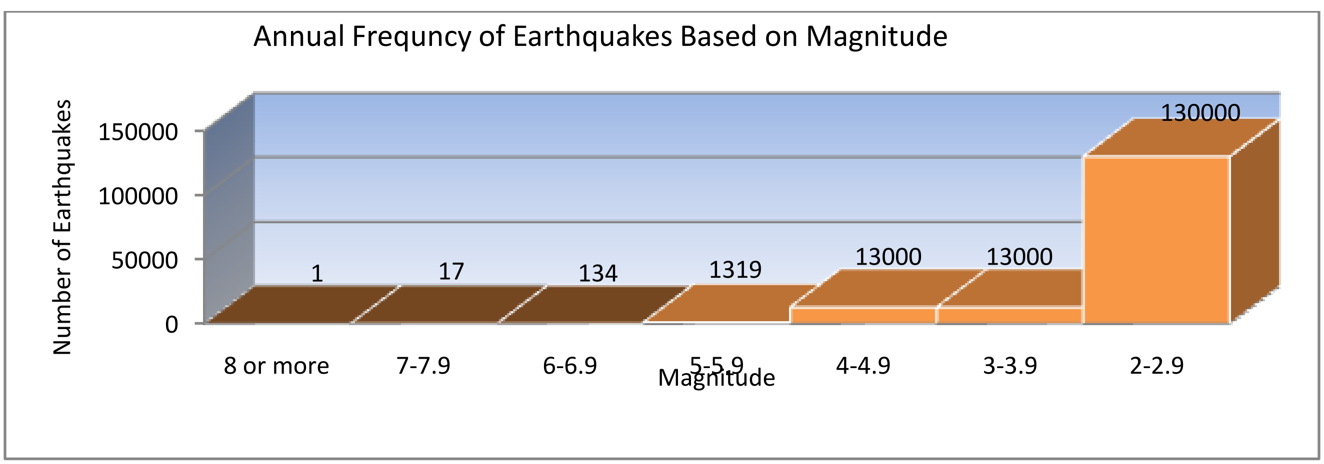

Figure 2: Annual Frequency of Earthquakes based on their Magnitude

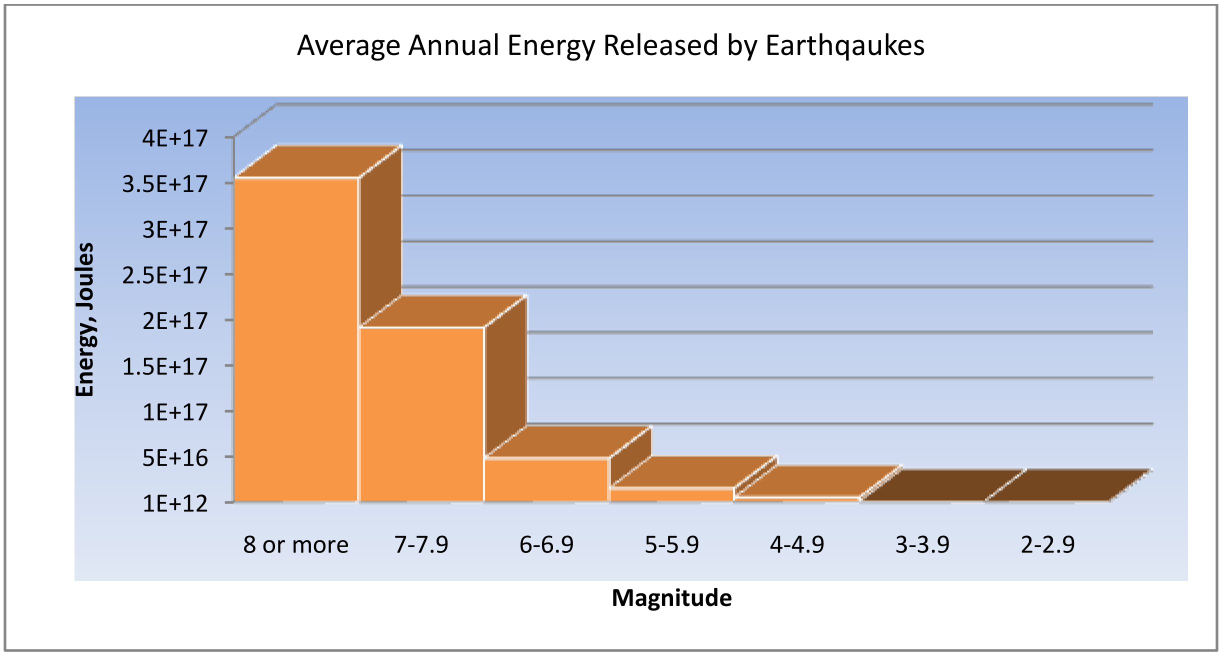

Figure 3: Average Annual Energy of Earthquakes based on their Magnitude

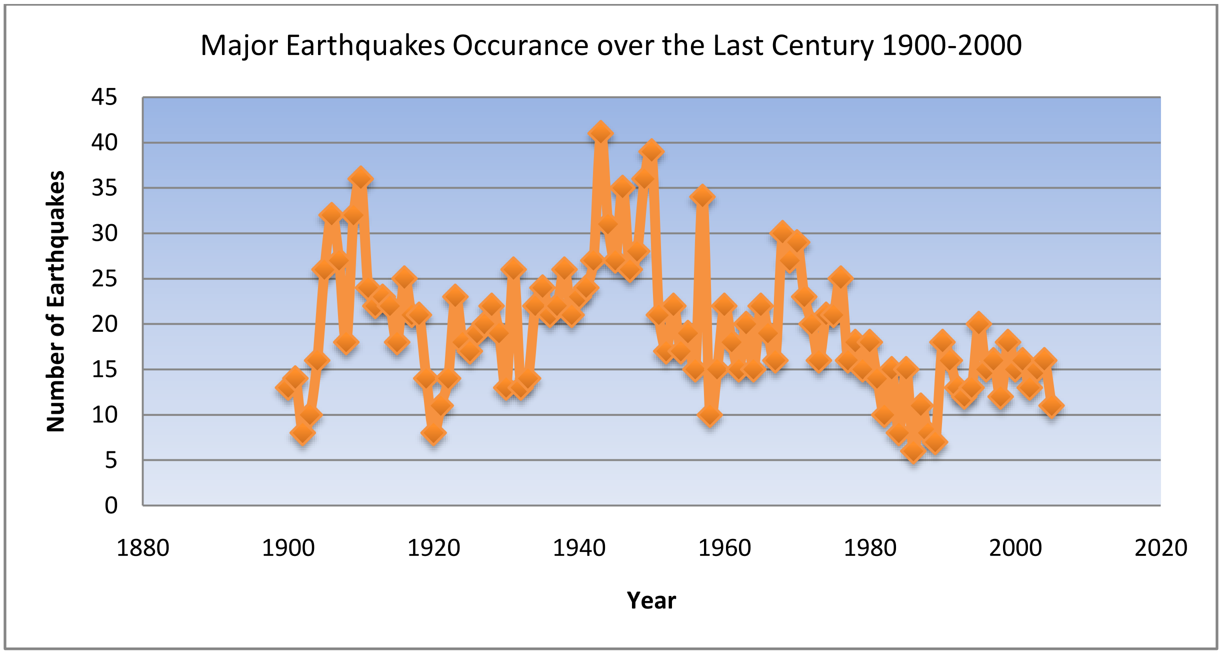

Figure 4: Major Earthquakes over the last century 1900-2000

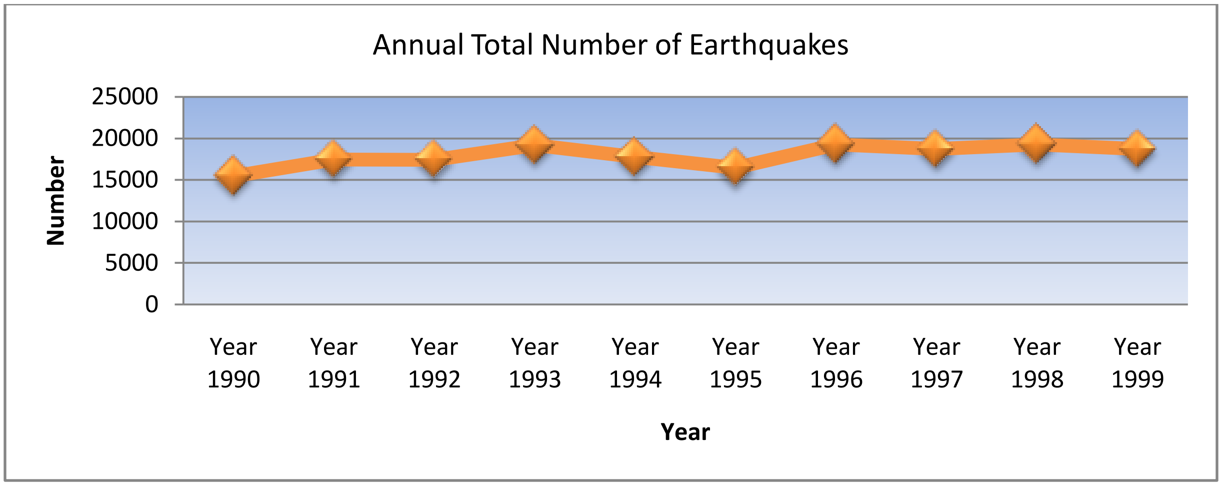

Figure 5: Total Annual Number of Earthquakes for Decade 1990-1999

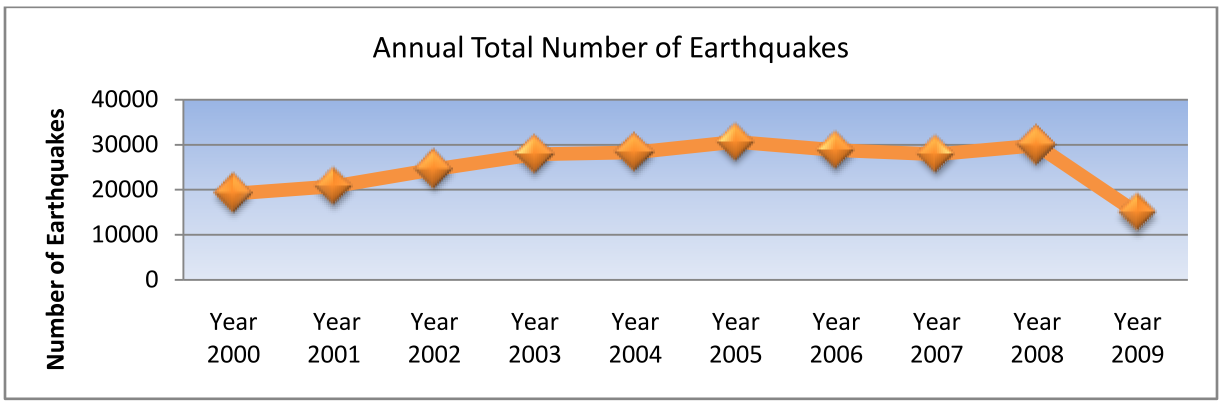

Figure 6: Total Annual Number of Earthquakes for Decade 2000-2009

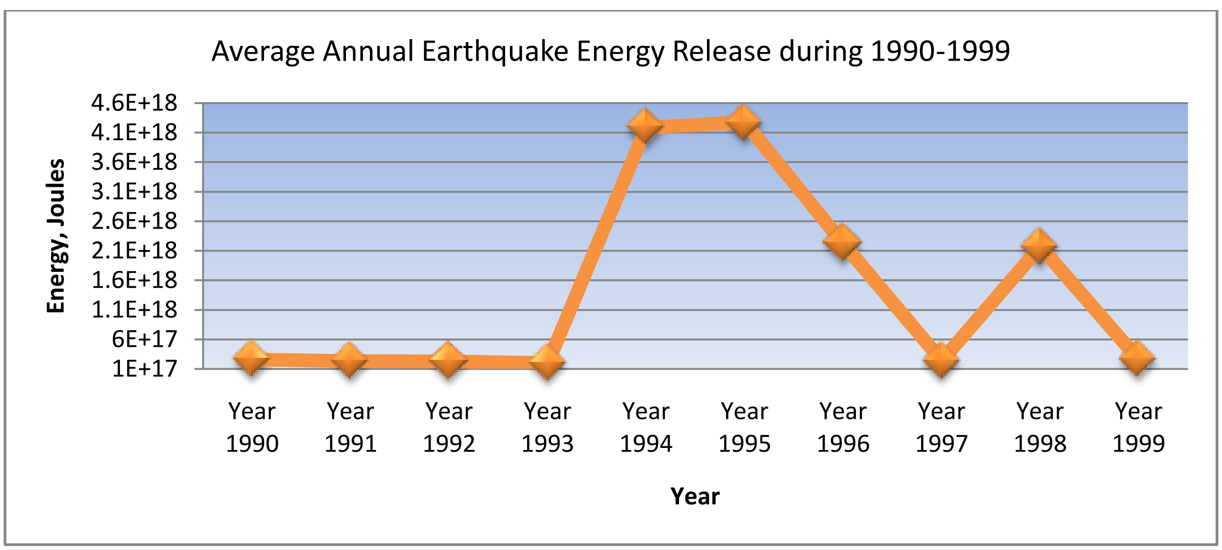

Figure 7: Average Annual Energy of Earthquakes form 1990-1999

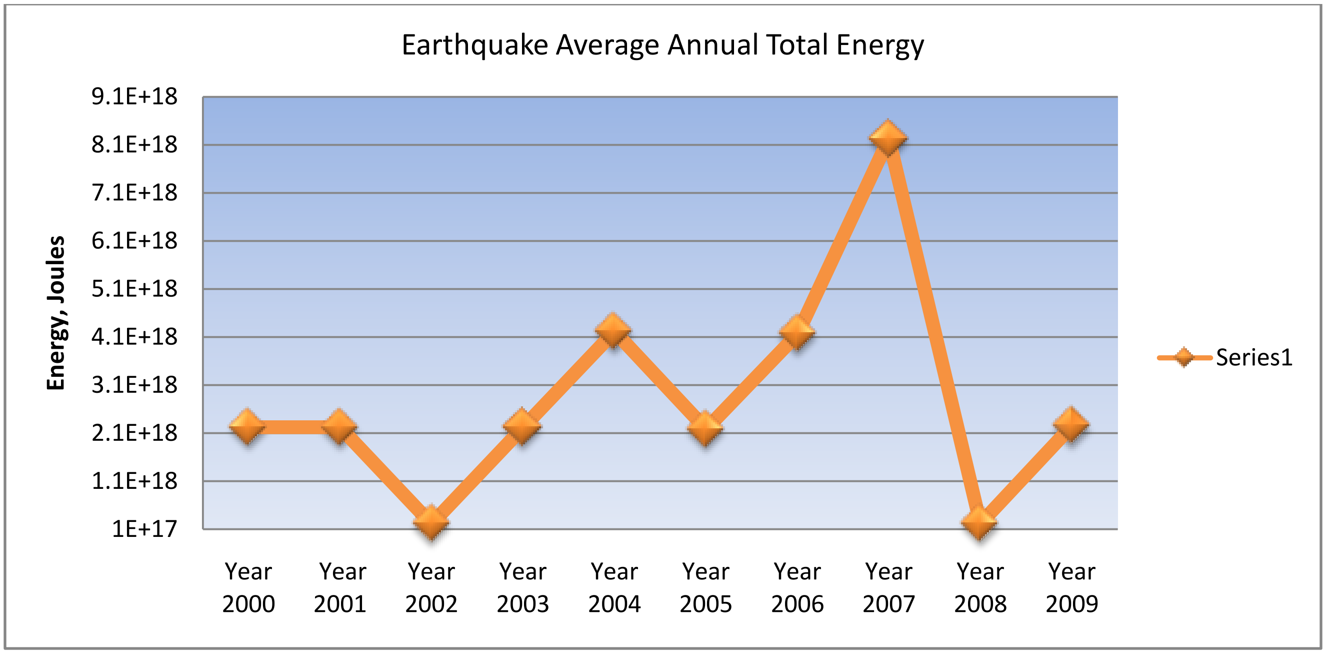

Figure 8: Average Annual Energy of Earthquakes form 2000-2009

IV. Data Analysis and ANFIS Results

The goal of earthquake prediction is to give warning of potentially damaging earthquakes early enough to allow appropriate response to the disaster, enabling people to minimize loss of life and property. A primary goal of earthquake research is to increase the reliability of earthquake probability estimates. Ultimately, scientists would like to be able to specify a high probability for a specific earthquake on a particular fault within a particular year. Scientists estimate earthquake probabilities in two ways: by studying the history of large earthquakes in a specific area and the rate at which strain accumulates in the rock.

Scientists study the past frequency of large earthquakes in order to determine the future likelihood of similar large shocks. For example, if a region has experienced four magnitude 7 or larger earthquakes during 200 years of recorded history, and if these shocks occurred randomly in time, then scientists would assign a 50 percent probability (that is, just as likely to happen as not to happen) to the occurrence of another magnitude 7 or larger quake in the region during the next 50 years. But in many places, the assumption of random occurrence with time may not be true, because when strain is released along one part of the fault system, it may actually increase on another part. Four magnitude 6.8 or larger earthquakes and many magnitude 6 to 6.5 shocks occurred in the San Francisco Bay region during the 75 years between 1836 and 1911. For the next 68 years (until 1979), no earthquakes of magnitude 6 or larger occurred in the region. Beginning with a magnitude 6.0 shock in 1979, the earthquake activity in the region increased dramatically; between 1979 and 1989, there were four magnitude 6 or greater earthquakes, including the magnitude 7.1 Loma Prieta earthquake. This clustering of earthquakes leads scientists to estimate that the probability of a magnitude 6.8 or larger earthquake occurring during the next 30 years in the San Francisco Bay region is about 67 percent (twice as likely as not).

Another way to estimate the likelihood of future earthquakes is to study how fast strain accumulates. When plate movements build the strain in rocks to a critical level, like pulling a rubber band too tight, the rocks will suddenly break and slip to a new position. Scientists measure how much strain accumulates along a fault segment each year, how much time has passed since the last earthquake along the segment, and how much strain was released in the last earthquake. This information is then used to calculate the time required for the accumulating strain to build to the level that results in an earthquake. This simple model is complicated by the fact that such detailed information about faults is rare. In the United States, only the San Andreas fault system has adequate records for using this prediction method.

This paper introduces an adaptive neural fuzzy inference system (ANFIS) approach to predict the location and magnitude of earthquakes. The analysis performed in this paper is based on the principle of conservation of energy and momentum of annual earthquakes. This principle shall not be violated due to the fact that the angular earth speed about its axis is fixed to keep the 24 hours daytime unchanged. Furthermore, it is assumed that the area under the moment curve of earthquakes in the north part of the earth balances the area under the moment curve in the south part of the earth. The data used in the analysis is obtained from USGS. For automatically tuning Sugeno-type inference systems, a sample of training data is used to train the ANFIS. In first training the earthquake ANFIS methodology, the location of the earthquake is used as an input, meanwhile the moment of the earth quake is assigned as the output. Furthermore, the earthquake ANFIS system is modified such that the location, magnitude and the timing of the earthquakes are given as inputs. The output ANFIS dynamic predictor was capable to predict historic earthquakes with high accuracy with a 0.17424 converging error. Dynamic ANFIS earthquake predictor along with 3D meshed surfaces are further introduced and found to be efficient as well. Finally, the ANFIS results are demonstrated to show the effectiveness of the approach.

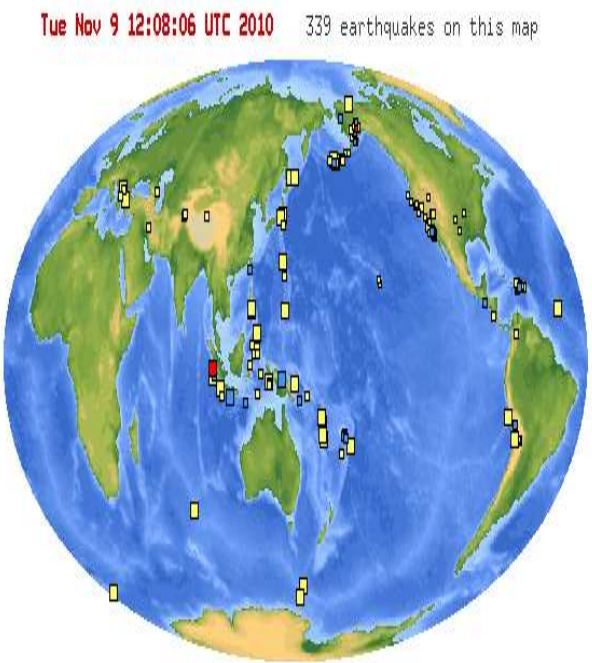

Figure 9: USGS Localization Earthquake on Nov. 9, 2010

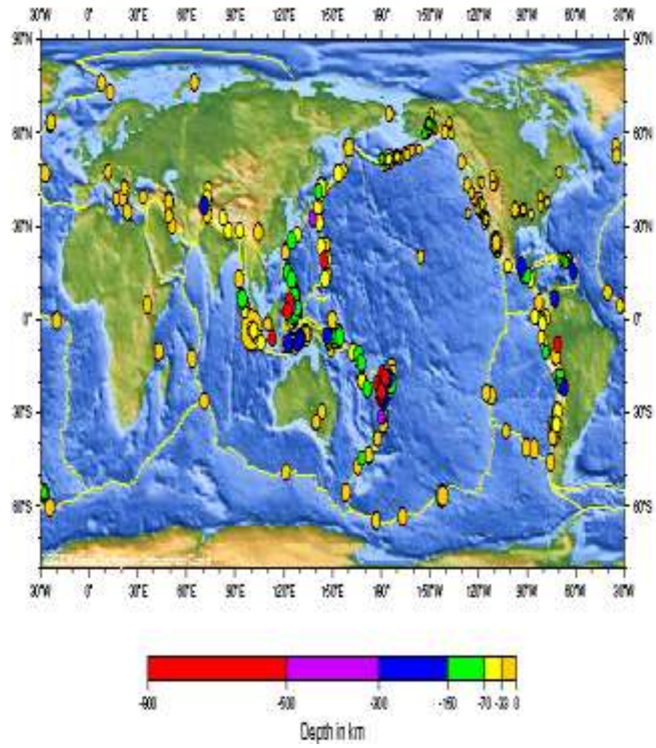

Figure 10: USGS Earthquakes Map from Oct. 18 to Nov.9, 2010

Figure 9 demonstrates the earthquakes on the planet as by Nov. 9, 2010. Meanwhile, Figure 10 localizes the occurrence of earthquakes three weeks before Nov. 9, 1001. It obvious to figure that earthquakes occur at the boundaries of tectonic plates and are concentrated at the intersection nodes. Basically those nodes serve as zero moment supports.

In this paper the analysis is performed based on the following facts and assumptions:

1. The conservation of angular momentum of Earth.
2. The steadiness of the annual frequency of earthquakes
3. The conservation of annual earthquakes energy
4. The moment of earthquakes occur in the north earth balances the moment of earthquakes occur in south earth
5. The intersection of tectonic nodes serves as zero moment supports.

A. Training Data Set 1 and ANFIS Results

The data provided by USGS listed in Appendix 1 represents the first set to train ANFIS. USGS data includes date of the earthquakes, latitude location, and magnitude. Using such information the corresponding energy and moment released by earthquakes are calculated using the formulas provided in section 3.

The moment diagram of the earthquakes under investigation is demonstrated in Figure 11. This shows that the moment of earthquakes in the north part should balance the moment of earthquakes in the south. As discussed in earlier sections, this compliers with the conservation of angular momentum of Earth to maintain a fixed duration of the day on the planet.

Here we apply fuzzy inference to an earthquake system for which a collection of input/output data has been recorded to use for modeling since there is no predetermined model of earthquake variable system.

The basic structure of fuzzy inference system seen in Figure 12 is a model that maps input characteristics to input membership functions, input membership function to rules, rules to a set of output characteristics, output characteristics to output membership functions, and the output membership function to a single-valued output or a decision associated with the output.

The neural adaptive learning method works similarly to that of neural networks. Neural adaptive learning techniques provide a method for the fuzzy modeling procedure to *learn* information about a data set. Then fuzzy Logic computes the membership function parameters that best allow the associated fuzzy inference system to track the given earthquake input/output data.

Using a given earthquake input/output data set, ANFIS constructs a fuzzy inference system (FIS) whose membership function parameters are tuned (adjusted) using either a backpropagation algorithm in combination with a least squares method. This adjustment allows fuzzy earthquake system to learn from the data to be modeled.

The parameters associated with the membership functions changes through the learning process. The computation of these parameters (or their adjustment) is facilitated by a gradient vector. This gradient vector provides a measure of how well the fuzzy inference system is modeling the input/output data for a given set of parameters. When the gradient vector is obtained, an optimization routines is applied in order to adjust the parameters to reduce some error measure. This error measure is defined by the sum of the squared difference between actual and desired outputs. More specifically. ANFIS uses either back propagation or a combination of least squares estimation and back-propagation for membership function parameter estimation.

Model validation is a process by which the input vectors from input/output data sets on which the FIS was not trained before, are presented to the trained FIS model, to check how well the FIS model predicts the corresponding data set output values. One problem with model validation for models constructed using adaptive techniques is selecting a data set that is both representative of the data the trained model is intended to emulate, yet sufficiently distinct from the training data set so as not to render the validation process trivial. Checking data will be used in the next section.

If a large amount of data is collected, hopefully this data contains all the necessary representative features, so the process of selecting a data set for checking or testing purposes will be easier.

The following figures shows the ANFIS structure (Figure 12), training data (Figure 13), FIS output (Figure 14), training error (Figure 15). ANFIS info: Number of nodes: 72, Number of linear parameters: 34, Number of nonlinear parameters: 34, Total number of parameters: 68, Number of training data pairs: 20, Number of checking data pairs: 0, Number of fuzzy rules: 17.

In Figure 12 colored branches characterize the rules and indicate whether or not *and*, *not*, or *or* are used in the rules. The input is represented by the left-most node and the output by the right-most node. The node represents a normalization factor for the rules.

Hybrid ANFIS Parameter optimization method is used for FIS training are hybrid (mixed least squares and back-propagation). Zero error tolerance is used to create a training stopping criterion with 270 epochs. The training will stop after the training data error remains within this tolerance. The training error converged to 0.83.

As it can be seen from Figure 14 and 15, ANFIS was successful to train all earthquake data to an error of .83. Furthermore the moment of each earthquake then has been tested by the FIS and high accuracy has been achieved as shown in Figure 16.

The predicted FIS output has been transformed into magnitude strength at Richter scale and then compared with the recorded value to calculate for the error. The error was zero for some values, with a minimum of -1 and maximum of 2.25. These results might be acceptable for low or medium earthquakes since it would not be catastrophic and not deconstructive.

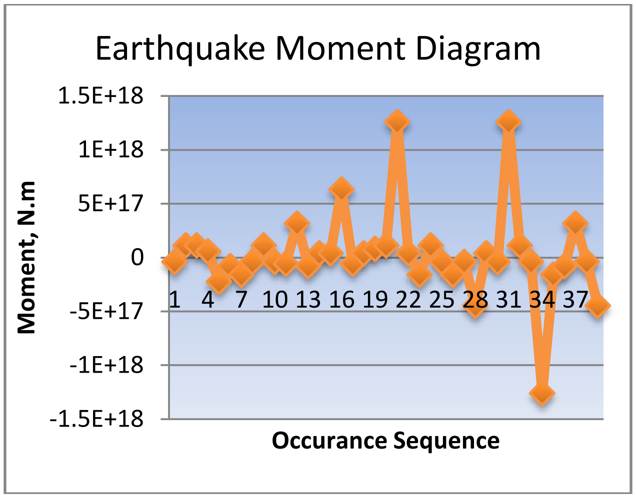

Figure 11: Moment Diagram (N.m)

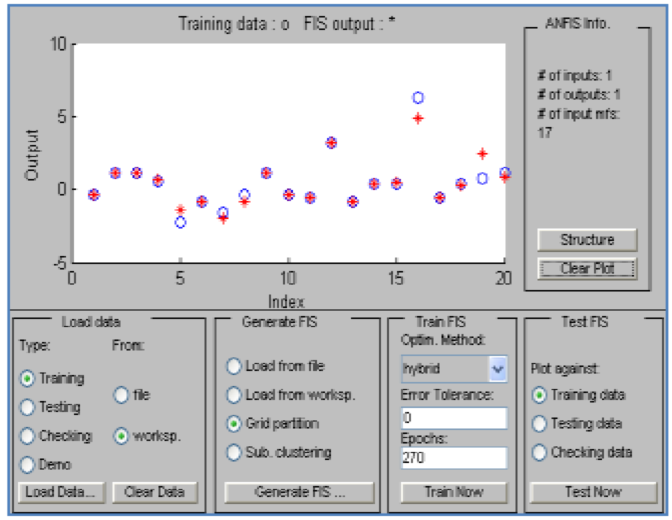

Figure 14: ANFIS Testing FIS

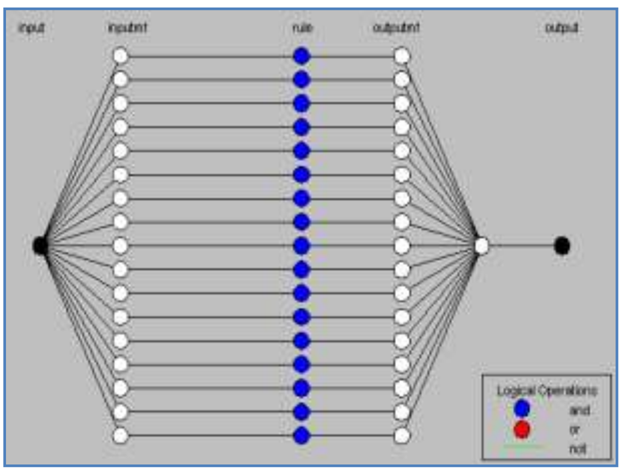

Figure 12: ANFIS Structure

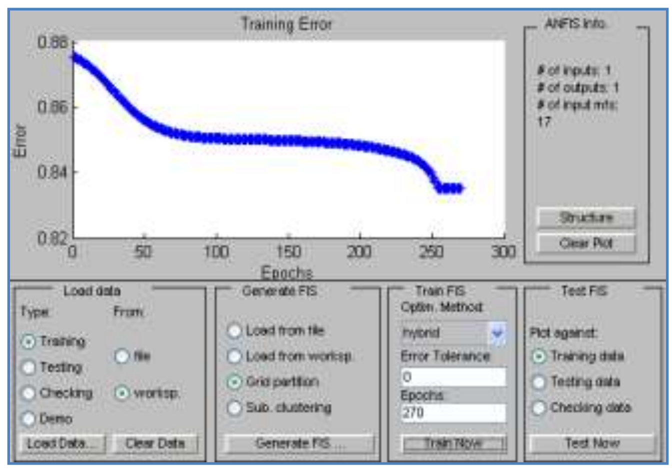

Figure 15: ANFIS Training Error

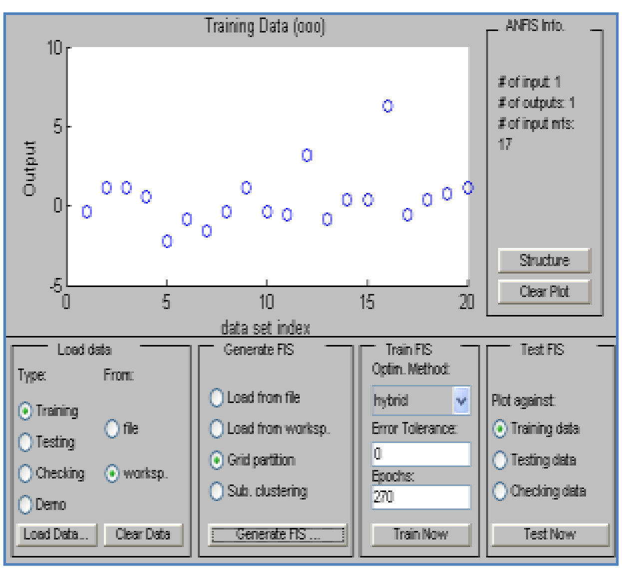

Figure 13: ANFIS Training Data

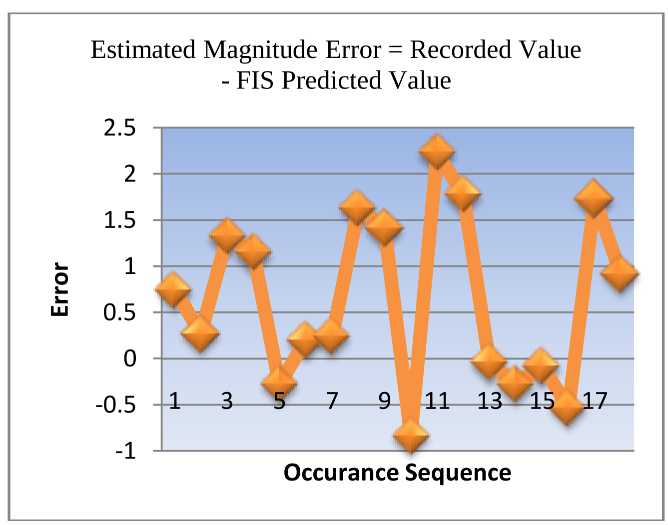

Figure 16: Magnitude Error

B. Training Data Set 2 and ANFIS Results

To enhance prediction of earthquakes several improvements have been followed in this section:

- To further test the complexty of ANFIS more, another set of data with more population has been used. The advantage of such training approach is that the number of inputs has increased such that it includes the latitude (North/South), longitude (East/West), time and the output is the moment of the earthquake. This brings more sophistication to the training as well as resulting in more accuracy and ability to predict locations and timing of earthquakes to occur.
- The checking data is used for testing the generalization capability of the fuzzy inference system at each epoch. The checking data has the same format as that of the training data, and its elements are generally distinct from those of the training data.
- The checking data is important for learning earthquakes for which the input number is larger and/or the data itself is noisy. A fuzzy inference system needs to track a given input/output data set well. A validation or checking data set can be useful for these situations. This data set is used to cross-validate the fuzzy inference model. This cross-validation requires applying the checking data to the model and then seeing how well the model responds to this data.
- Another advantage of the ANFIS approach is the Dynamic Predicting of the Moment of Earthquakes versus Locations. Using the dynamic curser, one can choose any location at any time to check what is the predicted earthquake moment. Note the time scale here is the accumulative days of each month of a given year starting with as 1 and counting on days of each month.
- The energy and moment released from the earthquakes occurred on the week Oct. 7-13,2010 is presented in Figure 17 and 18, respectively. The maximum jolted on Oct. 9.
- The FIS membership function parameters computed using both training and checking data are loaded are associated with the training epoch that has a minimum checking error. ANFIS info: Number of nodes: 78, Number of linear parameters: 108, Number of nonlinear parameters: 27, Total number of parameters: 135, Number of training data pairs: 90, Number of checking data pairs: 0, Number of fuzzy rules: 27. The following figures shows the ANFIS training data (Figure 23), training error (Figure 24), FIS output (Figure 25), Fuzzy Sugeno Network Structure (Figure 26), ANFIS Dynamic Output Predicting the Moment of Earthquakes versus Locations (Figure 27), and ANFIS Surface in Figures 28, 29 and 30.

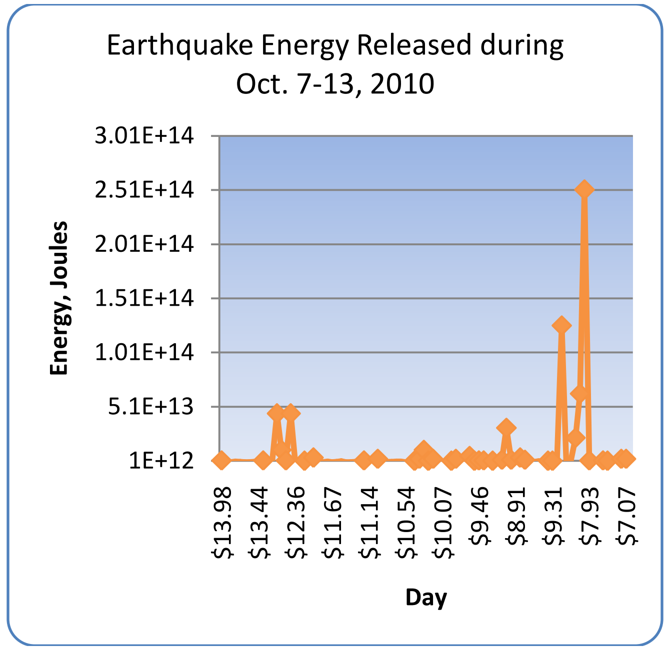

Figure 17: Earthquake Energy from Oct. 7-13, 2010

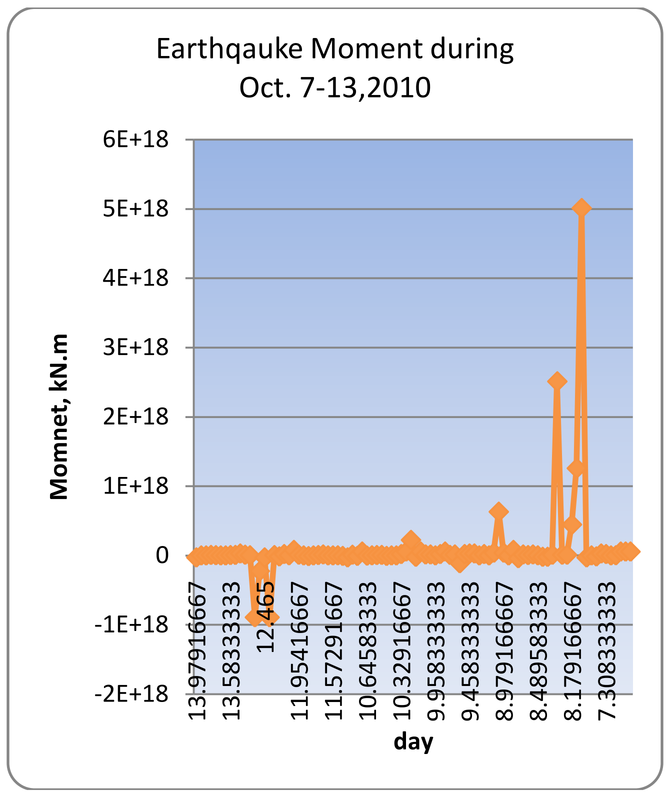

Figure 18: Earthquake Moment from Oct. 7-13, 2010

The basic structure of fuzzy inference system seen in Figure 19 is a model that maps input characteristics to input membership functions, input membership function to rules, rules to a set of output characteristics, output characteristics to output membership functions, and the output membership function to a single-valued output or a decision associated with the output. The ANFIS is composed of 5 layers, one for the input, one for the output, and three inner layers. These three layers: one for the input membership function followed by the rule layer and succeeded by the output membership function layer. In Figure 19 colored branches characterize the rules and indicate whether or not *and*, *not*, or *or* are used in the rules. The input is represented by the left-most node and the output by the right-most node. The node represents a normalization factor for the rules.

The parameters associated with the membership functions changes through the learning process. Figures 20, 21, 22 represent the membership functions of the FIS variables: time, latitude and logtitude, respectively. The computation of these parameters (or their adjustment) is facilitated by a gradient vector. This gradient vector provides a measure of how well the fuzzy inference system is modeling the input/output data for a given set of parameters.

This error measure is defined by the sum of the squared difference between actual and desired outputs. More specifically. Hybrid ANFIS Parameter optimization method is used for FIS training are hybrid (mixed least squares and back-propagation). Using a given earthquake input/output data set, ANFIS constructs a fuzzy inference system (FIS) whose membership function parameters are tuned (adjusted) using a backpropagation algorithm in combination with a least squares method shown in Figure 23. This adjustment allows fuzzy earthquake system to learn from the data to be modeled. Blue circles represent the original data and the red to represent the trained one.

Zero error tolerance is used to create a training stopping criterion with 277 epochs. Figure 24 shows that the training resulted error was 1.75. As it can be seen from Figure 25, ANFIS was successful to train all earthquake data to an error convergence of 0.17424.

Model validation is a process by which the input vectors from input/output data sets on which the FIS was not trained before, are presented to the trained FIS model, to check how well the FIS model predicts the corresponding data set output values as in Figure 26. One problem with model validation for models constructed using adaptive techniques is selecting a data set that is both representative of the data the trained model is intended to emulate, yet sufficiently distinct from the training data set so as not to render the validation process trivial. If a large amount of data is collected, hopefully this data contains all the necessary representative features, so the process of selecting a data set for checking or testing purposes will be easier. Checking data against the training data is shown in Figure 26. The major earthquakes have been validated with the same error although some data shows divergence.

Dynamic ANFIS earthquake predictor is shown in Figure 28. The advantage of this predictor is that a specific location (latitude and longitude) at given date can be selected to predict the earthquake moment strength (as scale factor is used 10^{17}) . The figure for example shows that a latitude 2.68 south and longitude 14.9 on day 10 (Oct. 16) the earthquake moment is $8.3x10^{17}$ N.m. On the other hand ANFIS earthquake moment surfaces are also so useful to have a 3D overview. For example, Figure 29 shows that the Latitude range 0 to 50 North will not suffer any earthquakes over the 16 days. Meanwhile south locations ranges from latitudes 0 to 50 will witness earthquakes. A maximum strength occurs at latitude 50 south on Oct. 7 and Oct. 23 with a moment force value of $1x10^{20}$ N.m. Inspecting Figure 30 predicts that on 60 latitude south and Longitude 180 west a strong earthquake occurs with moment strength of $8x10^{19}$ N.m. Checking Figure 31 yields that earthquakes activity is increasing in the locations 0 to 50 Latitudes south and 0 to 100 north longitudes.

Furthermore the moment of each earthquake then has been tested by the FIS and high accuracy has been achieved as shown in Figure 32. The predicted FIS output has been transformed into magnitude strength at Richter scale and then compared with the recorded value to calculate for the error. The error was zero for some values, with a minimum of -0.75 and maximum of 3. FIS is able to predict most of the exact earthquakes magnitudes with zero error.

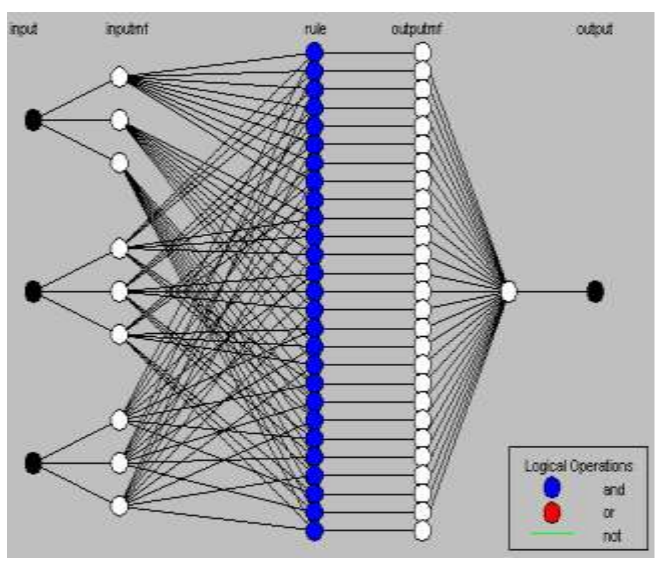

Figure 19: ANFIS Structure

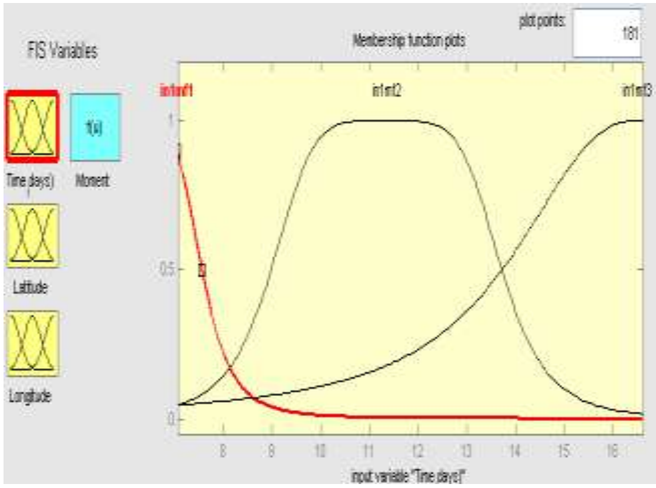

Figure 20: Membership Function of the FIS variable (Time)

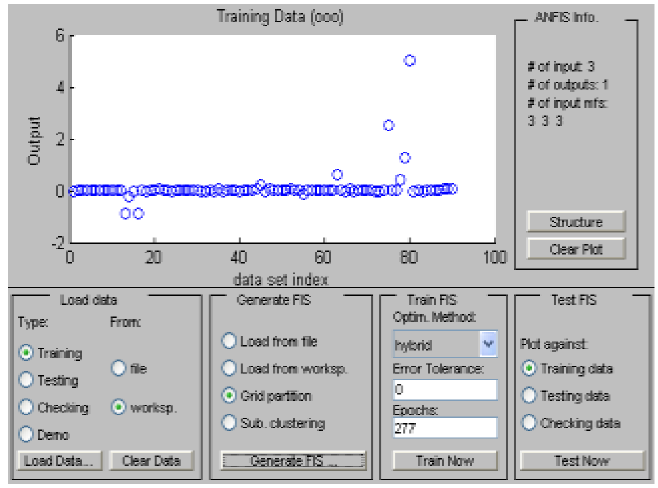

Figure 23: ANFIS Training Data

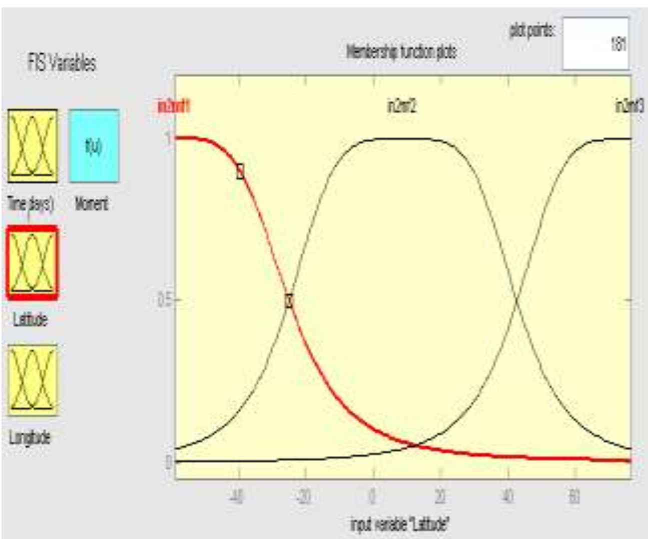

Figure 21: Membership Function of the FIS variable (Latitude)

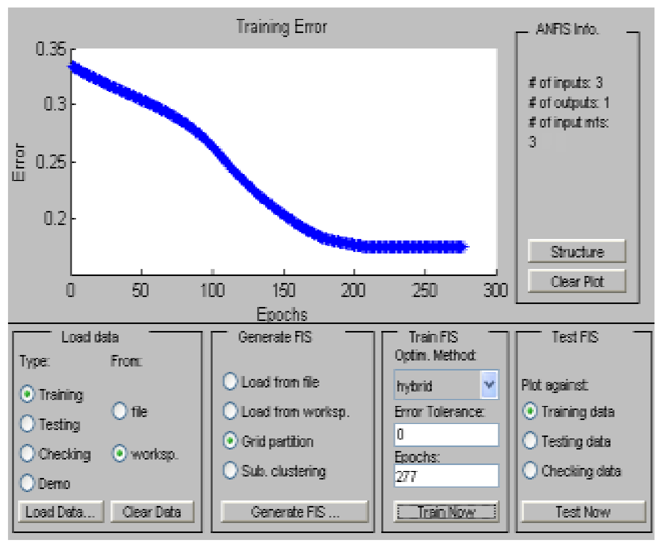

Figure 24: ANFIS Training Error

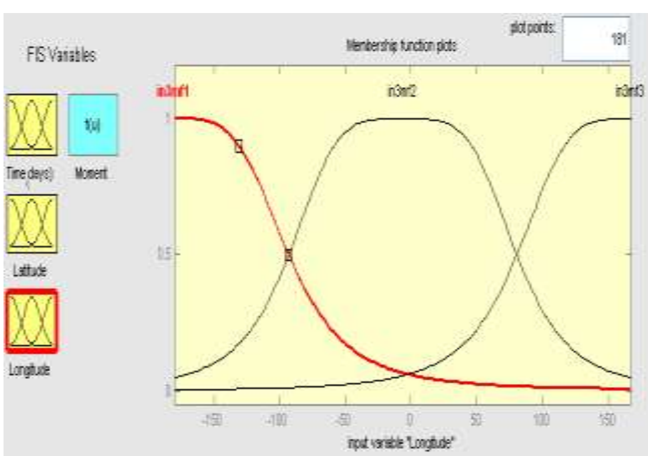

Figure 22: Membership Function of the FIS variable (Longitude)

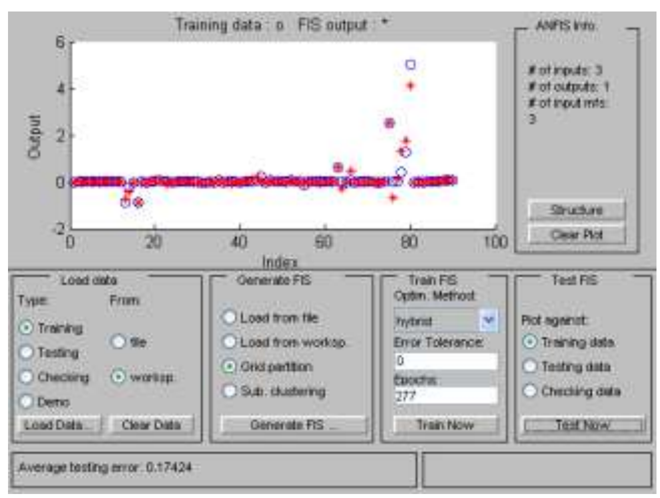

Figure 25: Training Data versus FIS Output

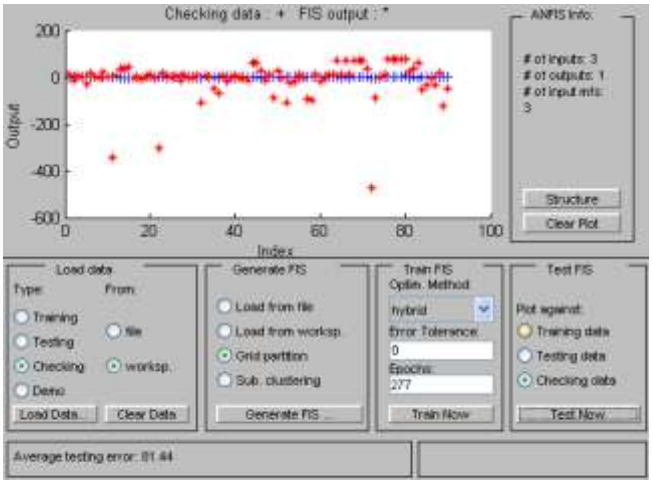

Figure 26: Checking Data versus FIS Output

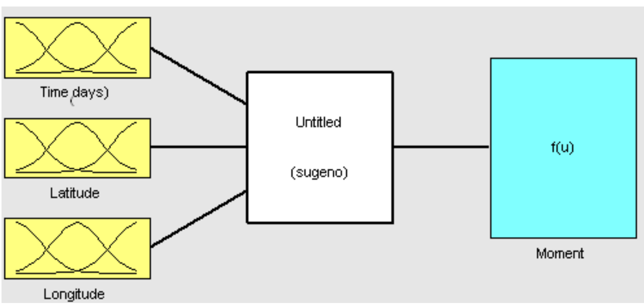

Figure 27: Fuzzy Sugeno Structure

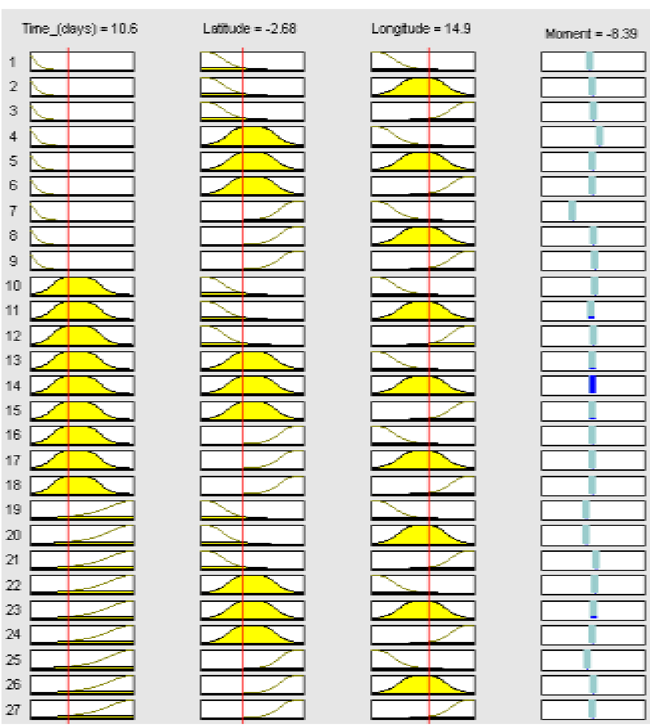

Figure 28: ANFIS Dynamic Output Predictor of the Moment of Earthquakes versus Time and Locations

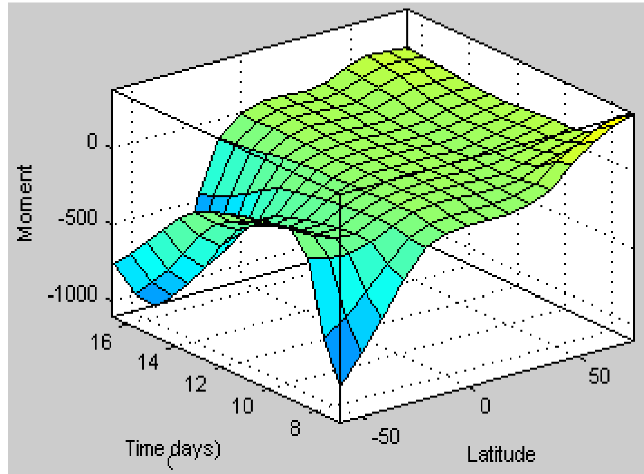

Figure 29: ANFIS Earthquake Surface: Time and Latitude versus Moment

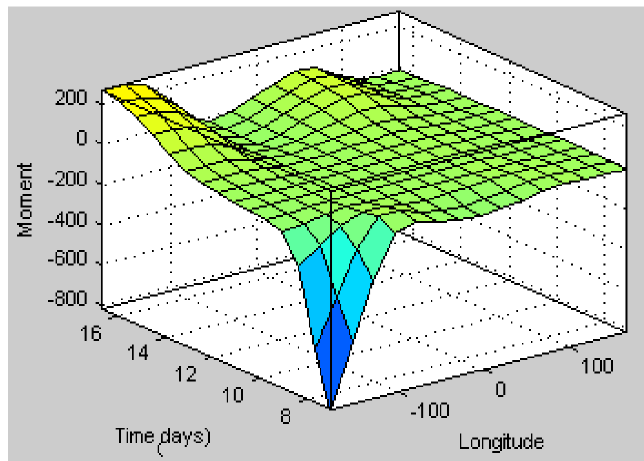

Figure 30: ANFIS Earthquake Surface: Time and Longitude versus Moment

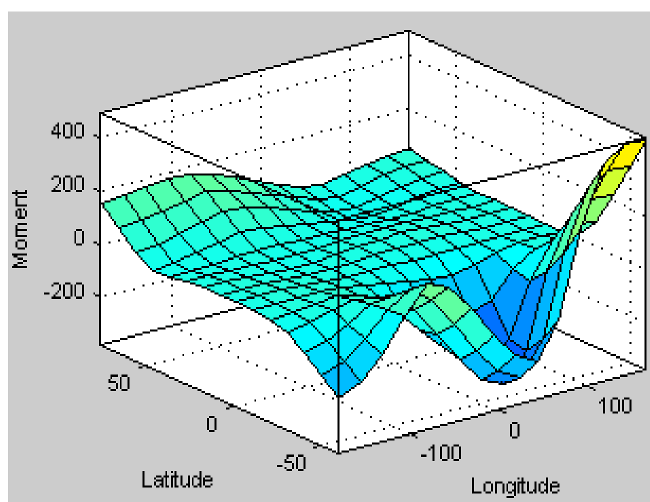

Figure 31: ANFIS Earthquake Surface: Latitude and Longitude Versus Moment

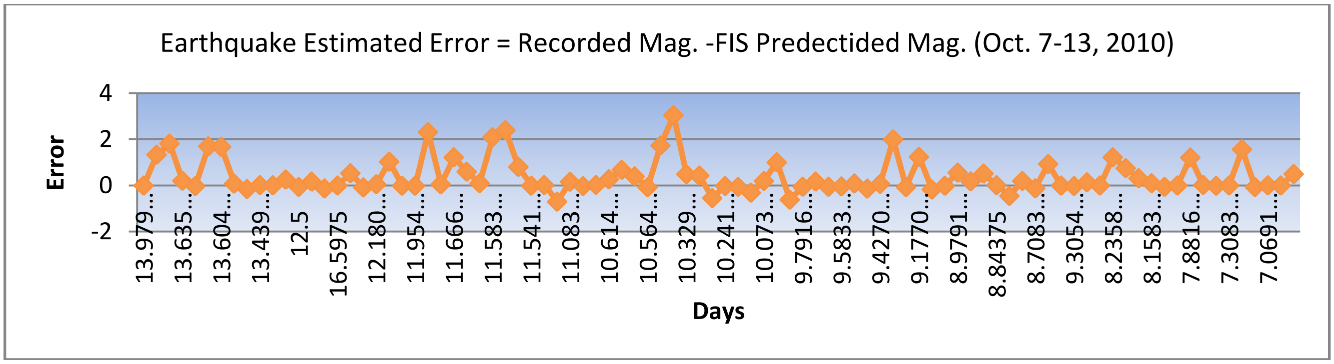

Figure 32: Magnitude Error = Recorded Magnitude – ANFIS Predicted Magnitude

V. Conclusions and Future Work

In this paper an adaptive neural fuzzy inference system (ANFIS) approach is introduced to predict the location and magnitude of earthquakes. The analysis performed in this paper is based on the principle of conservation of energy and momentum of annual earthquakes due to the fact that the 24-hour daytime is unchanged.

Two training data sets have been analyzed. In the first training the earthquake ANFIS methodology, the location of the earthquake is used as an input, meanwhile the moment of the earth quake is assigned as the output. The resulted training error was stabilized after 250 epochs converging to an acceptable value of 0.84. The data trained was for earthquakes occurred between April 12-15, 2010.

For the second training set recorded in the week Oct. 7-13, 2010, ANFIS system is modified such that the latitude, longitude locations, the occurrence time of the earthquakes are given as inputs where as the earthquake moment is the output. The advantage of such training approach is that the number of inputs has increased such that it includes the location (North/South), East/West, Time and the output is the moment force of the earthquake. This brings more sophistication to the training as well as resulting in more accuracy and ability to predict locations and timing of earthquakes to occur. Another advantage of the ANFIS approach is the Dynamic Output Predictor of the Moment of Earthquakes versus Locations and date. Using the dynamic curser, one can choose any location at any time to check what would be the next predicted earthquake moment force value. This value then can converted to Richter magnitude using moment-magnitude formula given by (14). Additionally, ANFIS Surfaces are found also to be so useful to have a 3D earthquake overview.

Future work will extend this work to train ANFIS for the Entire year long as well as for recorded decades. To improve the ANFIS training results, considering also the depth of the earthquake as additional input will add more representation of the nature of earthquakes. Designing a real-time mechatronics earthquake predictor will also have a valuable impact on saving people’s lives and reduce catastrophic destructions.

References

[1] United States Geological Survey’s (USGS), www. earthquake.usgs.gov.

[2] “Earthquake Energy Rise on Earth”, Tom J. Chalko, NU Journal of Discovery, May 2008.

[3] Chuji Tsoubi, “Energy accounts of earthquakes in and near Japan,”. Journal of Phys. Earth. Vol. 41, 1965.

[4] “The Energy Release in Great Earthquakes,” Hiroo Kanamori, Journal of Geophysical Research, Vol 88, No. 20, 1977.

[5] “Magnitude 8.8 Offshore Maule, CHILE,” IRIS, USGS, 2010.

[6] “Relationships Among Magnitudes and Seismic Moment of Earthquakes in the Taiwan Region,” Kou-Cheng Chen1, Win-Gee Huang, and Jeen-Hwa Wang, Terr. Atmos. Ocean. Sci., Vol. 18, No. 5, 951-973, December 2007.

[7] Huang Chongfu, Shi Peijun and Zhang Yuanming, Fuzzy mathematical method of Urban Natural Hazard and Risk Assessment, Bulletin for Studies and Exchanges on Fuzzines and its Applications, Vol 59, 93-98, 1994.

[8] “ANFIS: Adaptive-Network-Based Fuzzy Inference System”, J.S.R. Jang, *IEEE Trans. Systems, Man, Cybernetics*, 23(5/6):665-685, 1993.

[9] “Neuro-Fuzzy Modeling and Control”, J.S.R. Jang and C.-T. Sun, *Proceedings of the IEEE*, 83(3):378-406

[10] *The Fuzzy Logic Toolbox for use with MATLAB*, J.S.R. Jang and N. Gulley, Natick, MA: The MathWorks Inc., 1995.

[11] *Machine Learning, Neural and Statistical Classification* Michie, Spiegelhart & Taylor (Eds.), NY: Ellis Horwood 1994.

[12] *www.nasa.gov*

[13] Xian-Bo He, Li Yang, Xian-hua Zeng, Gang-yuan Zhang, Xing-qiang Zhao, "An Adaptive Fuzzy Scheduling and Fuzzy-PID Performance Control Model Suitable for Soft Real-time Systems," International Journal of Computer Information Systems and Industrial Management Applications (IJCISIM), Vol.1 , pp.287-294, 2009.

[14] Patrick Marques Ciarelli, Elias Oliveira, Claudine Badue and Alberto Ferreira De Souza, "Multi-Label Text Categorization Using a Probabilistic Neural Network," International Journal of Computer Information Systems and Industrial Management Applications (IJCISIM), Vol.1, pp.133-144, 2009.

[15] Tanish Zaveri, Ishit Makwana, Mukesh Zaveri, "Novel Hybrid Multispectral Image Fusion Method using Fuzzy Logic," International Journal of Computer Information Systems and Industrial Management Applications (IJCISIM), Vol.2, pp.096-103.

Appendix 1: Training Data for Week April 12-17, 2010 (Provided by USGS)

Date	Latitude Location	Magnitude	Energy (J)	Moment (N.m)
4/17/2010 16:00	-7.035	5	1.99526E+12	3.98107E+16
4/17/2010 10:02	3.638	5.3	5.62341E+12	1.12202E+17
4/17/2010 7:23	3.667	5.3	5.62341E+12	1.12202E+17
4/17/2010 0:59	32.588	5.1	2.81838E+12	5.62341E+16
4/16/2010 23:15	-37.374	5.5	1.12202E+13	2.23872E+17
4/16/2010 22:44	-23.725	5.2	3.98107E+12	7.94328E+16
4/16/2010 22:41	-37.279	5.4	7.94328E+12	1.58489E+17
4/16/2010 22:38	-37.484	5	1.99526E+12	3.98107E+16
4/16/2010 10:01	16.606	5.3	5.62341E+12	1.12202E+17
4/16/2010 8:58	-8.919	5	1.99526E+12	3.98107E+16
4/16/2010 3:01	-10.657	5.1	2.81838E+12	5.62341E+16
4/16/2010 1:45	54.588	5.6	1.58489E+13	3.16228E+17
4/15/2010 13:40	-31.206	5.2	3.98107E+12	7.94328E+16
4/14/2010 8:16	31.799	5	1.99526E+12	3.98107E+16
4/14/2010 5:16	18.204	5	1.99526E+12	3.98107E+16
4/14/2010 1:25	33.179	5.8	3.16228E+13	6.30957E+17
4/14/2010 1:16	-29.052	5.1	2.81838E+12	5.62341E+16
4/14/2010 0:18	17.971	5	1.99526E+12	3.98107E+16
4/14/2010 0:12	33.159	5.2	3.98107E+12	7.94328E+16
4/14/2010 0:01	32.875	5.3	5.62341E+12	1.12202E+17
4/13/2010 23:49	33.224	6	6.30957E+13	1.25893E+18
4/13/2010 21:40	33.183	5	1.99526E+12	3.98107E+16
4/13/2010 20:27	-56.259	5.4	7.94328E+12	1.58489E+17
4/13/2010 20:14	8.091	5.3	5.62341E+12	1.12202E+17
4/13/2010 15:46	-10.86	5	1.99526E+12	3.98107E+16
4/13/2010 0:55	-4.396	5.4	7.94328E+12	1.58489E+17
4/12/2010 12:36	-35.356	5	1.99526E+12	3.98107E+16
4/12/2010 10:23	-56.917	5.7	2.23872E+13	4.46684E+17
4/12/2010 7:57	76.939	5	1.99526E+12	3.98107E+16
4/12/2010 5:51	-4.582	5	1.99526E+12	3.98107E+16

Appendix 2: Training Data for Week Oct. 7-13, 2010 (Provided by USGS)					
10/13/2010 23:32	13.85S	167.79E	75	4.9	VANUATU
10/13/2010 18:39	43.07N	110.84W	11	2.8	WYOMING
10/13/2010 15:51	63.22N	137.88W	10	2.6	SOUTHERN YUKON TERRITORY, CANADA
10/13/2010 15:13	12.57N	88.14W	66	4.5	OFFSHORE EL SALVADOR
10/13/2010 15:07	33.25N	48.99E	10	4.3	WESTERN IRAN
10/13/2010 14:45	61.07N	150.93W	11	2.8	SOUTHERN ALASKA
10/13/2010 14:27	32.24N	115.41W	13	2.9	BAJA CALIFORNIA, MEXICO
10/13/2010 14:06	35.19N	97.32W	13	4.4	OKLAHOMA
10/13/2010 10:36	51.60N	173.14W	24	4.5	ANDREANOF ISLANDS, ALEUTIAN IS.
10/13/2010 5:59	13.97N	146.66E	25	4.9	MARIANA ISLANDS REGION
10/13/2010 5:40	73.06N	12.93E	14	4.6	NORWEGIAN SEA
10/13/2010 2:17	4.43N	32.51W	10	4.2	CENTRAL MID-ATLANTIC RIDGE
10/12/2010 12:02	20.48S	173.98W	12	5.9	TONGA
10/12/2010 12:01	20.36S	174.23W	10	5.5	TONGA
10/12/2010 11:10	20.02S	177.61W	270	4.9	FIJI REGION
10/12/2010 10:21	4.91S	133.67E	13	5.9	NEAR S COAST OF PAPUA, INDONESIA
10/12/2010 8:47	6.71N	72.95W	172	4.4	NORTHERN COLOMBIA
10/12/2010 7:01	21.13S	68.52W	97	4.7	ANTOFAGASTA, CHILE
10/12/2010 4:20	2.64N	122.15E	540	4.8	CELEBES SEA
10/12/2010 3:00	32.20N	115.29W	6	4.1	BAJA CALIFORNIA, MEXICO
10/11/2010 23:16	25.35N	124.78E	109	5.2	NORTHEAST OF TAIWAN
10/11/2010 22:48	76.25N	64.78E	10	4.6	NOVAYA ZEMLYA, RUSSIA
10/11/2010 16:58	32.28N	115.36W	1	2.9	BAJA CALIFORNIA, MEXICO
10/11/2010 16:33	24.42S	179.83W	506	4.6	SOUTH OF THE FIJI ISLANDS
10/11/2010 16:06	35.31N	92.33W	6	3.6	ARKANSAS
10/11/2010 14:11	14.57N	92.57W	56	4.4	OFFSHORE CHIAPAS, MEXICO
10/11/2010 14:10	41.12N	141.26E	108	4.7	HOKKAIDO, JAPAN REGION
10/11/2010 13:57	37.15N	117.38W	11	2.6	NEVADA
10/11/2010 13:43	35.29N	92.34W	7	2.5	ARKANSAS
10/11/2010 13:33	35.30N	92.31W	6	4	ARKANSAS
10/11/2010 13:00	4.81S	133.98E	6	4.5	NEAR THE SOUTH COAST OF PAPUA, INDONESIA
10/11/2010 8:35	33.79S	71.75W	38	4.9	VALPARAISO, CHILE
10/11/2010 3:17	19.10N	144.86E	615	4.6	MAUG ISLANDS REG, N. MARIANA IS.
10/11/2010 2:07	8.23S	120.28E	39	4.5	FLORES REGION, INDONESIA
10/10/2010 21:44	33.94N	72.84E	33	5.1	PAKISTAN
10/10/2010 15:32	30.73S	178.30W	77	4.3	KERMADEC ISLANDS, NEW ZEALAND
10/10/2010 14:56	2.53N	95.81E	38	4	SIMEULUE, INDONESIA
10/10/2010 14:47	35.58N	140.85E	5	4.4	NEAR THE EAST COAST OF HONSHU, JAPAN
10/10/2010 13:50	15.31N	61.45W	151	4.5	DOMINICA REGION, LEEWARD ISLANDS
10/10/2010 13:35	6.35S	129.88E	177	4.5	BANDA SEA
10/10/2010 12:48	35.32N	92.33W	5	3	ARKANSAS
10/10/2010 11:10	35.31N	92.31W	4	1.8	ARKANSAS
10/10/2010 7:53	31.04N	141.76E	44	4.8	IZU ISLANDS, JAPAN REGION
10/10/2010 6:25	51.48N	175.18W	35	5.1	ANDREANOF ISLANDS, ALEUTIAN IS.
10/10/2010 6:08	51.46N	175.26W	33	5.5	ANDREANOF ISLANDS, ALEUTIAN IS.
10/10/2010 5:48	23.32S	179.83W	550	4.8	SOUTH OF FIJI ISLANDS
10/10/2010 2:27	31.06N	141.61E	14	5.1	IZU ISLANDS, JAPAN REGION
10/10/2010 2:10	0.84N	85.18W	53	4.7	OFF COAST OF ECUADOR
10/10/2010 1:41	39.28N	72.44E	61	4.7	TAJIKISTAN

10/9/2010 23:03	30.90N	115.65W	11	3.7	BAJA CALIFORNIA, MEXICO
10/9/2010 21:46	25.84N	127.77E	30	4.8	RYUKYU ISLANDS, JAPAN
10/9/2010 19:04	38.16N	22.74E	11	5.1	GREECE
10/9/2010 18:36	48.28N	154.13E	81	4.5	KURIL ISLANDS
10/9/2010 17:19	55.19N	160.06E	38	4.7	KAMCHATKA PENINSULA, RUSSIA
10/9/2010 14:04	2.65S	76.60W	123	5.3	PERU-ECUADOR BORDER REGION
10/9/2010 13:16	26.20N	144.51E	22	4.8	BONIN ISLANDS, JAPAN REGION
10/9/2010 10:58	38.78N	72.88E	10	4.9	TAJIKISTAN
10/9/2010 10:15	39.28N	70.22E	15	4.9	TAJIKISTAN
10/9/2010 7:42	32.92N	100.88W	5	3.1	WESTERN TEXAS
10/9/2010 6:12	35.81N	140.44E	29	4.8	NEAR EAST COAST OF HONSHU, JAPAN
10/9/2010 4:13	35.30N	92.32W	5		ARKANSAS
10/9/2010 3:25	18.24N	146.48E	72	5	PAGAN REG., N. MARIANA ISLANDS
10/9/2010 1:54	10.21N	84.29W	91	5.8	COSTA RICA
10/8/2010 23:32	51.15N	174.99W	25	5	ANDREANOF ISLANDS, ALEUTIAN IS.
10/8/2010 21:45	1.66N	126.61E	64	4.5	MOLUCCA SEA
10/8/2010 21:22	51.29N	175.18W	28	5.2	ANDREANOF ISLANDS, ALEUTIAN IS.
10/8/2010 20:16	13.88S	49.22W	10	5	TOCANTINS-GOIAS BORDER REGION, BRAZIL
10/8/2010 18:28	51.27N	175.07W	27	4.7	ANDREANOF ISLANDS, ALEUTIAN IS.
10/8/2010 17:44	51.30N	175.08W	5	4.4	ANDREANOF ISLANDS, ALEUTIAN IS.
10/8/2010 17:00	58.75N	152.63W	56	4.7	KODIAK ISLAND REGION, ALASKA
10/8/2010 11:45	31.21N	115.89W	10	4	BAJA CALIFORNIA, MEXICO
10/8/2010 10:15	58.83S	25.59W	10	4.8	SOUTH SANDWICH ISLANDS REGION
10/8/2010 7:21	33.68S	72.03W	16	4.8	OFFSHORE VALPARAISO, CHILE
10/8/2010 6:47	25.94N	124.39E	181	4.6	NORTHEAST OF TAIWAN
10/8/2010 5:43	2.83N	128.22E	116	6.2	HALMAHERA, INDONESIA
10/8/2010 5:40	51.25N	175.24W	37	4.6	ANDREANOF ISLANDS, ALEUTIAN IS., ALASKA
10/8/2010 4:28	51.19N	175.19W	28	4.6	ANDREANOF ISLANDS, ALEUTIAN IS., ALASKA
10/8/2010 4:19	51.33N	175.20W	7	5.7	ANDREANOF ISLANDS, ALEUTIAN IS., ALASKA
10/8/2010 3:49	51.28N	175.18W	28	6	ANDREANOF ISLANDS, ALEUTIAN IS., ALASKA
10/8/2010 3:26	51.37N	175.36W	19	6.4	ANDREANOF ISLANDS, ALEUTIAN IS.
10/7/2010 22:17	5.15S	151.46E	137	4.9	NEW BRITAIN REGION, P.N.G.
10/7/2010 21:10	32.59N	115.75W	3	3.4	BAJA CALIFORNIA, MEXICO
10/7/2010 20:04	20.59S	178.44W	550	4.7	FIJI REGION
10/7/2010 9:11	33.49N	90.80E	8	4.9	XIZANG-QINGHAI BORDER REGION
10/7/2010 7:25	53.47N	160.35E	49	4.8	NEAR THE EAST COAST OF KAMCHATKA, RUSSIA
10/7/2010 4:09	18.08N	66.95W	22	2.5	PUERTO RICO
10/7/2010 3:41	42.20N	137.52E	291	4.2	EASTERN SEA OF JAPAN
10/7/2010 1:42	1.03N	124.39E	188	5.1	MINAHASA, SULAWESI, INDONESIA
10/7/2010 1:40	39.15N	70.28E	4	5.1	TAJIKISTAN
10/7/2010 1:21	28.67N	66.07E	10	4.6	PAKISTAN

Author Biography

Murad Shibli joined the United Arab Emirates University (UAEU) since 2008 as a visiting assistant Professor. Before Joining UAEU the author worked for one year at American University of Sharjah. The author served as a founding chair of the Mechatronics Mechatronics departme-nt at the German Jordanian University from 2006-2007. As a graduate Ph.D. student from Concordia University in Montréal Canada his graduate research focused on modeling and control of free-flying space robotic systems.